ARTICLE IN PRESS

Ceramics International xxx (xxxx) xxx–xxx

Contents lists available at ScienceDirect

Ceramics International

journal homepage: www.elsevier.com/locate/ceramint

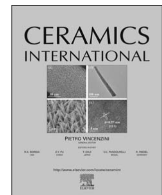

Evolution of material removal modes of sapphire under varied scratching depths

Jinhu Wang, Bing Guo*, Qingliang Zhao, Chunyu Zhang, Quanli Zhang, Wenjie Zhai

Center for Precision Engineering, School of Mechatronics Engineering, Harbin Institute of Technology, Harbin 150001, China

ARTICLE INFO

Keywords:
Sapphire
Scratching
Plastic deformation
Brittle fracture
Acoustic Emission

ABSTRACT

Scratching experiments were conducted on C-plane of sapphire along the [01$\bar{1}$0] direction to investigate the evolution of material removal modes under varied scratching depths. The results indicated that the material removal experienced three stages depending on the increase of scratching depth. Pure plastic flow was firstly observed as the scratching depth was small enough, characterized by smooth scratching groove, curled shavings and tiny stick-slip lines. Plastic deformation and brittle fracture coexisted in the second stage, where the initial radial cracks, tearing and segmental chips appeared. Brittle fracture dominated in the final stage: irregular debris and spalling occurred due to the intersection of lateral and radial cracks. In addition, the mechanism of plastic deformation and the cracks initiation/evolution of sapphire is discussed by combining the scratching patterns with the contact-induced deformation theory. Finally, the scratching-induced Acoustic Emission (AE) signals were processed based on fast Fourier transform and wavelet packet decomposition. The characteristics of the AE signals corresponding to the three material removal stages are discussed in frequency domain.

1. Introduction

Sapphire is a promising high-performance transparent material for many optical applications, such as visible/infrared windows and optical lenses that exposed to harsh environments [1,2]. However, the extremely high hardness and brittleness of sapphire make it difficult to obtain defect-free surfaces. The surface/subsurface damages induced by brittle fracture would reduce sapphire's strength and increase the subsequent polishing time [3]. Therefore, the material removal mode, brittle or ductile, plays a vital role in quality control of the machined surface. An investigation on the evolution of the material removal modes from plastic flow to brittle fracture under scratching can provide primary information on the machining surface damage mechanism and make it possible to better control the machining process.

Extensive researches on the deformation and fracture behaviors of sapphire provided valuable information about the anticipated deformation systems, the onset of plasticity and the incipient fracture patterns [4–7]. The evidence of slip and twinning has been widely recognized, especially the twinning-dominated yield point mechanism, which appeared consistent with the experimental observations and the theoretical models [8–11]. Nowak et al. [12–14] summarized the available slip/twinning systems of sapphire and proposed a new model based on the effective resolved shear stress to estimate the probability to activate the slip/twinning systems. The calculation based on this model illustrated that the rhombohedral twinning has the highest probability during indentation on C-plane, followed by basal twinning [15]. However, due to the limited slip/twinning systems available, the main deformation mechanism of sapphire in macro-scale scratching tests is brittle fracture [16]. The propagation of cracks in sapphire is mainly along the well-defined crystal orientations [17]. Haney and Subhash [18] found that the crack orientations caused by indentation on C- and A-planes were consistent with the surface traces of R- and C-planes. Schmid and Harris [19] reported that the *c*-axis compression caused twinning on R-planes and the intersection of twins on different R-planes caused fracture. To produce satisfactory components of high surface integrity, ductile material removal should be achieved along each crystal orientation [20]. The brittle-ductile transition during the material removal process is affected by the material properties, indenter shapes, processing parameters, etc. [21–24]. For instance, a higher scratching velocity leads to a higher proportion of plastic deformation [25], and a larger brittle-ductile transition threshold could be achieved by the elliptical ultrasonic assisted scratching [26]. Although the indentation and scratching studies on sapphire have provided useful information on the material plastic deformation and brittle fracture, the mechanism of material removal transition from plastic flow to brittle fracture are far from being fully understood, and the characteristics in each stage of transition under scratching is rarely discussed.

* Correspondence to: Harbin Institute of Technology, P.O. Box 413, Harbin 150001, China.
E-mail address: guobing@hit.edu.cn (B. Guo).

http://dx.doi.org/10.1016/j.ceramint.2017.05.069
Received 2 March 2017; Received in revised form 9 May 2017; Accepted 9 May 2017
0272-8842/ © 2017 Published by Elsevier Ltd.

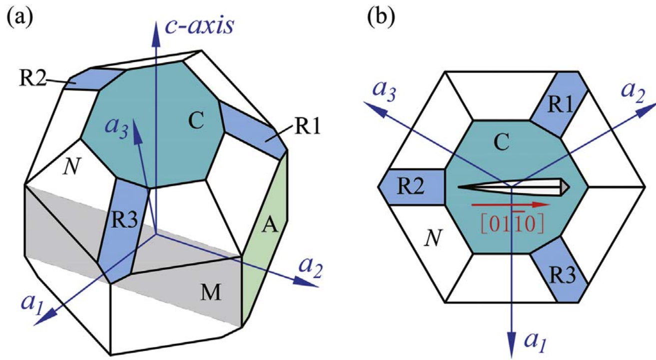

Fig. 1. The spatial location of the investigated crystal orientation: (a) the coordinate system and crystal geometry showing the crystal planes of sapphire; (b) the investigated scratching direction and its orientation in crystal.

In the present work, a Vickers pyramidal indenter is adopted as single abrasive grit and three series of scratching tests are performed under different scratching depths, including constant scratching depths in ductile and brittle regimes, as well as increasing scratching depths that result in material removal transiting from ductile to brittle regimes. The morphology of the scratching grooves and the components of the AE signals are then analyzed to investigate the mechanism of ductile-brittle transition and the respective characteristics of different material removal modes.

2. Material and methods

As illustrated in Fig. 1(a), all crystal planes of sapphire are defined relative to the C-plane which is the plane of physical and optical symmetry. A-planes and M-planes are all perpendicular to C-plane, while R-planes and N-planes is located at 57.6° and 51° relative to C-plane, respectively. For simplicity, the R-planes of ($\bar{1}$102), (0$\bar{1}$12) and (10$\bar{1}$2), were marked as R1, R2 and R3, respectively. The rhombohedral twinning on the R1-, R2- and R3-planes was denoted as R1-twinning, R2-twinning and R3-twinning, respectively, and the basal twinning was abbreviated as B-twinning in discussion. Due to the inherent anisotropy of sapphire, the strength, hardness and thermal properties vary considerably depending on the crystal orientation. In this study, the commercially available synthetic sapphire (Aurora Optoelectronics Co., Ltd. China) was used and the scratching experiments were performed along the [01$\bar{1}$0] direction on C-plane, as indicated by the red arrow line in Fig. 1(b). The sapphire specimen was prepared in a diameter of 25 mm and a thickness of 5 mm, and it was polished progressively using the diamond slurry (9 μm, 3 μm and 1 μm) until no obvious defects could be found under an optical microscope at 100× magnification.

The scratching tests were conducted with a Vickers pyramidal indenter on an ultra-precision grinding machine (see Fig. 2). The detailed experimental conditions are listed in Table 1. As shown in Fig. 2(a), the indenter is rigidly fixed to an arbor which is connected to the tool spindle. The force sensor is connected with the specimen by an adapter plate, and the AE sensor is mounted under the specimen to detect the indenter-specimen contact for tool setting and signal acquisition, as illustrated in Fig. 2(b). The scratching direction was kept parallel to one of the indenter diagonals. Three series of scratching tests, including varied and constant scratching depths, were performed without coolant addition. The scratches with linearly increasing scratching depths were obtained by z and y axes linkage, as illustrated in Fig. 2(c). The maximum scratching depths range from 0.25 μm to 3 μm with a fixed increment of 0.25 μm. The other two series of scratches were performed with constant maximum scratching depths of 0.5 μm and 2.5 μm, respectively. The detailed scratching parameters are listed in Table 2. The morphology of the scratching grooves, including the chips, cracks and spalling pits, was examined by a scanning electron microscope (SEM). The AE signal was analyzed by power spectrum and wavelet packet decomposition.

3. Results and discussion

3.1. Scratching patterns under increasing scratching depths

Although brittle fracture is the main surface feature for machining of hard and brittle materials, pure plastic flow can be obtained if the undeformed chip thickness is small enough. As shown in Fig. 3(a) and (b), the material removal is mainly in ductile regime under the scratching depths of 0.24 μm and 0.73 μm, which can be identified by the smooth scratching grooves and the long shavings. Specifically, the localized shear flow resulted in curled shavings ejected from the scratches. The surfaces of the scratching grooves and the shavings are smooth and covered with tiny stick-slip lines, indicating that the stick-slip mechanism occurred during the scratching process. Moreover, tiny cracks (indicated by the black arrows in Fig. 3(b)) form at the side of the scratching groove as the scratching depth is up to 0.73 μm, but the observed chips of about 0.76 μm thickness (shown in Fig. 3(c)) indic ates that the material removal was conducted mainly in ductile region. The material deformation is influenced by both the external causes, such as the indenter shape, process parameters, etc. [27–29], and the intrinsic factors, including internal defects and crystal structure. The activation of internal defects and the accumulation of slip/twinning on specific crystal planes within the material should account for the formation of tiny cracks.

Although the critical temperature causing brittle-ductile transition in Al_2O_3 is higher than $0.5T_M$ ($T_M \approx 2000$ ℃ is the melting temperature) [30], the scratching-induced high hydrostatic stress under the indenter can result in the plastic deformation of sapphire at much lower temperatures [31]. Besides, the mechanical strength of sapphire, especially the *c*-axis compression strength, decreases rapidly as the temperature increases up to > 400 °C [19]. Therefore, the scratching-induced high hydrostatic stress and local temperature rising are the two external motivations of plastic flow. In addition, plastic deformation of sapphire is essentially accomplished by the accumulation of slip/twinning during the scratching process, which occurs when the stress on the indenter-specimen contact surface exceeds the yield strength but below the fracture strength. The activation of slip/twinning systems depends on the resolved shear stress (RSS) τ, which is expressed as follows:

$$\tau = \sigma \cdot \cos\lambda \cos\varphi \tag{1}$$

where σ is the average compressive stress on the indenter-specimen contact surface, λ is the angle between the force vector $\boldsymbol{F}$ (perpendicular to the indenter face) and the normal vector of the slip plane $\boldsymbol{n}$, and φ is the angles between $\boldsymbol{F}$ and the slip direction $\boldsymbol{g}$, as illustrated in Fig. 4. The probability T_i that activates the ith slip/twinning system is given by Eq. (2) [12,13]:

$$T_i(\mu) \propto \frac{\tau_i}{\tau_{CRi}/\min \tau_{CRi}} \cdot \Lambda_i \tag{2}$$

where μ is the angle determining the orientation of the indenter face on the surface of the crystal, $\tau_{CRi}/\min\tau_{CRi}$ is the relative critical shear stress (RCSS), which refers to the ratio of the critical shear stress for the ith slip/twinning system and the minimum of all possible critical shear stresses. The constraint factor Λ_i denotes the orientation of the indented crystal plane, which is described as follows:

$$\Lambda = \cos\omega \cos\delta \tag{3}$$

where ω is the angle between the vector $\boldsymbol{K}$ (along the intersection of the plane determined by the vectors $\boldsymbol{n}$, $\boldsymbol{g}$ with the plane of indenter face) and the vector $\boldsymbol{G}$ (along the projection of the pyramid axis on the indenter face), and δ is the angle determined by $\boldsymbol{G}$ and $\boldsymbol{g}$, as shown in Fig. 4. According to Eqs. (1)–(3) and the RCSS summarized in Ref.

Download English Version:

https://daneshyari.com/en/article/5437706

Download Persian Version:

https://daneshyari.com/article/5437706

Daneshyari.com